Journal of Materials Chemistry B

ROYAL SOCIETY OF CHEMISTRY

PAPER

View Article Online
View Journal | View Issue

Cite this: J. Mater. Chem. B, 2024, 12, 8767

Purpose-built multicomponent supramolecular silver(I)-hydrogels as membrane-targeting broad-spectrum antibacterial agents against multidrug-resistant pathogens†

Ekata Saha, [ab] Afruja Khan,[c] Amirul Islam Mallick*[c] and Joyee Mitra *[ab]

Received 21st June 2024,
Accepted 29th July 2024

DOI: 10.1039/d4tb01355g

rsc.li/materials-b

Membrane-targeting compounds are of immense interest to counter complicated multi-drug resistant infections. However, the broad-spectrum effect of such compounds is often unmet due to the surges of antibiotic resistance among majority of Gram-negative bacteria compared to Gram-positive species. Though amphiphiles, synthetic mimics of antimicrobial peptides *etc*, have been extensively explored for their potential to perturb bacterial membranes, small molecule-based supramolecular hydrogels have remained unexplored. The design of supramolecular hydrogels can be tuned on-demand, catering to desired applications, including facile bacterial membrane perturbation. Considering the strong biocidal properties of Ag-based systems and the bacterial membrane-targeting potential of appended primary amine groups, we designed self-assembled multicomponent supramolecular Ag(I)-hydrogels with urea and DATr (3,5-diamino-1,2,4-triazole) as ligands, which are predisposed for hydrogen bonding and interacting with negatively charged bacterial membranes at physiological pH. The synthesized supramolecular Ag(I)-hydrogels exhibited almost similar antibacterial activity against both Gram-negative (*Campylobacter jejuni*; *C. jejuni*) and Gram-positive (*Staphylococcus aureus*; *S. aureus*) bacteria, with minimal inhibitory concentration (MIC) of ~60 μg mL^{-1}. Ag(I)-hydrogels facilitated the disruption of the negatively charged bacterial membrane due to electrostatic interaction and complementary hydrogen bonding facilitated by DATr and urea. Sustained intracellular ROS generation in the presence of Ag(I)-hydrogel further expedited cell lysis. We envisage that the multicomponent supramolecular Ag(I)-hydrogels studied herein can be employed in designing effective antibacterial coatings on a range of medical devices, including surgical instruments. Moreover, the present form of the hydrogels has the potential to improve the antibacterial functionality of conventional antimicrobials, thus revitalizing the effective targeting of hard-to-treat multi-drug-resistant (MDR) bacterial infections in a clinical set up.

Introduction

The global rise of antimicrobial drug resistance among bacterial pathogens is a major cause of a delayed healing process, subsequent treatment failure and patient death worldwide, necessitating the development of novel antibacterial formulations, especially in the post-pandemic scenario.[1–3] Traditional treatment approaches are often associated with over-prescription and injudicious use of antibiotics, exacerbating the risk of emerging antibiotic resistance among common pathogens. A large number of antibiotics are rendered ineffective owing to the outer membrane barrier in both Gram-positive and Gram-negative pathogenic strains. The bacterial cell membrane is essential in maintaining cellular homeostasis, transporting nutrients and waste, and cellular respiration.[4] Thus, compounds targeting the bacterial membrane have garnered recent interest in countering multi-drug resistance (MDR).[4]

To this end, the antimicrobial activity of a range of membrane-targeting complexes has been assessed in the past, among which amphiphiles, synthetic mimics of antimicrobial peptides (AMR), are of note.[5–7] However, low molecular weight gelator (LMWG)-based supramolecular hydrogels have remained largely unexplored in this regard.[8] Supramolecular hydrogels and xerogels are employable as antibacterial coatings on surgical instruments or other medical devices. The available

[a] Inorganic Materials & Catalysis (IMC) Division, CSIR-Central Salt & Marine Chemicals Research Institute, Gijubhai Badheka Marg, Bhavnagar-364002, Gujarat, India. E-mail: joyeemitra@csmcri.res.in, joyeemitra@gmail.com
[b] Academy of Scientific and Innovative Research (AcSIR), AcSIR Headquarters, CSIR-HRDC Campus, Ghaziabad-201002, UP, India
[c] Department of Biological Sciences, Indian Institute of Science Education and Research Kolkata, Mohanpur, Nadia, West Bengal-741246, India. E-mail: amallick@iiserkol.ac.in

† Electronic supplementary information (ESI) available. See DOI: https://doi.org/10.1039/d4tb01355g

literature suggests the applications of hydrogels in wound dressings, antibacterial coatings of medical equipment, and implants.[9–12] Supramolecular hydrogels can be easily synthesized and more importantly, their activity can be customized by introducing multifunctionality and self-healability to further substantiate their applicability as antimicrobial coatings and dressings.[8] Recent reports reveal the promising antibacterial activity of triazole[13,14] and urea-derivatives[15,16] against infections caused by ESKAPE pathogens (*Enterococcus faecium*, *Staphylococcus aureus*, *Klebsiella pneumoniae*, *Acinetobacter baumannii*, *Pseudomonas aeruginosa*, and *Enterobacter* spp.) including methicillin-resistant *Staphylococcus aureus* (MRSA).

Hydrogels have emerged as an interesting therapeutic candidate in biomedical research due to their biocompatibility, high water content, and ability to drive the sustained release of active species as well as drugs to counter drug-resistant pathogens.[17] Supramolecular hydrogels with multiple hydrogen bond donor and acceptor centres have the additional potential to disrupt the polymeric bacterial cell membrane.[5] Primary amines are known to interact with the negatively charged bacterial membrane under physiological pH,[18] which led us to select 3,5-diamino-1,2,4-triazole (DATr) and urea as gelators for the attempted synthesis of multicomponent hydrogels.

Bactericidal effects of Ag nanoparticles (Ag(0)) have been extensively explored against Gram-positive and Gram-negative bacteria,[19–21] though the antibacterial effect arises due to the oxidation of Ag(0) to Ag(I) and its subsequent release.[22–24] However, Ag(I)-based systems have been relatively less explored.[25,26] There are distinct scopes for employing stable, multicomponent Ag(I)-hydrogels as a broad-spectrum antibiotic alternative against MDR pathogens. DATr is known to stabilize Ag(I) in complexes and does not allow its reduction under ambient conditions.[13] Considering these advantages, we designed supramolecular multicomponent Ag(I)-hydrogels employing an elegant combination of urea and DATr as ligands, owing to the abundance of primary amine groups and the possibility to participate in extensive hydrogen bonding interactions with the bacterial membrane.

To explore the broad-spectrum antibacterial efficacy of the fabricated Ag(I)-hydrogels, we selected two MDR bacteria, Gram-negative (*Campylobacter jejuni*) and Gram-positive (*Staphylococcus aureus*), as model pathogens. Among them, *Campylobacter jejuni* (*C. jejuni*) is a common gut pathogen associated with acute, self-limited gastrointestinal illness with several extra-intestinal autoimmune disorders, including Guillain–Barre syndrome (GBS), reactive arthritis, and inflammatory bowel disease.[27,28] While diarrheal cases of *Campylobacter* origin can be treated with macrolide antibiotics, the emergence of MDR *C. jejuni* isolates has left us with limited treatment options.[29] No vaccine is available except for biosecurity measures to prevent zoonotic transmission of *C. jejuni* to humans. On the other hand, we chose methicillin-resistant *Staphylococcus aureus* (MRSA) as a Gram-positive bacteria.[15,16] *Staphylococcus aureus* (*S. aureus*) is known as an opportunistic ESKAPE pathogen that can silently evade the host immune defence and ubiquitously colonize almost any niche throughout the human body.[30] By releasing an array of toxins and enzymes, *S. aureus* causes complicated nosocomial infections responsible for ~20–80% of global nosocomial infections.[31,32] In addition, *S. aureus* infection can cause pneumonia, osteomyelitis, meningitis, toxic shock syndrome, endocarditis and septicemia.[33,34]

In the present study, we observed marked growth inhibition of both the model pathogens, *C. jejuni* and *S. aureus*, in the presence of the Ag(I)-hydrogels. As expected, perturbation of the bacterial membrane was found to be substantial for both *C. jejuni* and *S. aureus*, following the treatment with Ag(I)-hydrogels. Our results attested to an almost similar efficacy of the hydrogels against *C. jejuni* and *S. aureus*, which is promising considering the challenges to develop a broad-spectrum antibiotic owing to the higher intrinsic antibiotic resistance among most Gram-negative bacteria compared to Gram-positive ones.[35] We surmise that the disruption of the bacterial membrane integrity owing to a combination of the positive zeta potential of the Ag(I)-hydrogels and extensive hydrogen bonding in the presence of appended $-NH_2$ groups in the gelator played a pivotal role in the observed broad-spectrum antibacterial activity of the hydrogels. Cell death was further triggered by the sustained production and intracellular accumulation of reactive oxygen species (ROS).[36] Together, the present study suggests that carefully tuned Ag(I)-hydrogels can be a promising alternative to broad-spectrum antibiotics in targeting hard-to-treat MDR and ESKAPE bacterial infections in a clinical setup.

Experimental section

Synthesis of AgDU-Gel1

DATr (0.5 mmol, 0.05 g) and urea (0.5 mmol, 0.03 g) were dissolved in water (0.5 mL) in a 5 mL glass vial upon slight warming. A solution of silver triflate, *i.e.* AgOTf (0.5 mmol, 0.128 g) in water (0.5 mL), was separately prepared and added to the ligand solution. Next, the mixture was stirred at room temperature for about 10 minutes to obtain a white-colored viscoelastic gel (**AgDU-Gel1**). The as-prepared **AgDU-Gel1** was then lyophilized under vacuum to obtain the corresponding xerogel **AgDU-Xero1**.

Synthesis of AgDU-Gel2

AgDU-Gel2 was prepared using a method similar to **AgDU-Gel1**, using a solution of silver nitrate, *i.e.* $AgNO_3$ (0.5 mmol, 0.085 g) in water (0.5 mL) instead of AgOTf. **AgDU-Gel2** was lyophilized similar to **AgDU-Gel1** to obtain the corresponding xerogel **AgDU-Xero2**.

Biological studies

C. jejuni TGH 9011 strain (BEI Resources, USA) was grown in Mueller Hinton (MH) broth (HiMedia, India) for 24 h under microaerophilic conditions (10% CO_2, 5% O_2, and 85% N_2) at 37 °C in a tri-gas incubator (Thermo Fisher Scientific, USA). An MRSA strain of *S. aureus* (a kind gift from Dr Samiran Bandyopadhyay, IVRI Eastern Regional Station, Belgachia, Kolkata) was grown in Luria-Bertani (LB) broth media (HiMedia) under constant shaking at 37 °C for 24 h in a BOD incubator.

Details of biological experiments have been provided as ESI.†

Statistical analysis

The GraphPad Prism statistical software (version 8) was used for graphical presentations and data analysis. The CC_{50} of the test compounds was calculated using a nonlinear regression curve. A Shapiro–Wilk test was performed to confirm the normal distribution. The Student *t*-test (two-tailed, unpaired) or nonparametric Mann–Whitney *U* test was performed to compare significance among various experimental groups. $^{*}P \leq 0.05$ and $^{**}P \leq 0.01$ were considered statistically significant.

Results and discussion

Synthesis and characterization of Ag(I)-hydrogels

Systematic screening and selection of metal precursors, organic ligands, and solvent systems are essential for supramolecular metallogel formation. A lukewarm aqueous solution of DATr and urea in equimolar proportions reacted with an aqueous solution of Ag(I) precursors (AgOTf or $AgNO_3$ *i.e.* **AgDU-Gel1** and **AgDU-Gel2**, respectively) to form a white-colored hydrogel at room temperature (RT) (Fig. 1). The gelation state was ascertained as the hydrogel sustained its own weight upon the 'inversion of the glass vial'. The gelation was not observed in the absence of Ag(I) salts. The hydrogels were stable on standing overnight at RT, and for several days upon refrigeration (4–10 °C). From the mass spectral pattern, we anticipate that the basic repeating unit for the gels is a dimeric Ag(I) species, which is bridged by two DATr ligands. The ring nitrogen atoms are preferred for metal coordination, as these are better donors than the exocyclic $-NH_2$ moieties. The urea ligand serves as a linker between such units and is responsible for the propagation of the Ag–DATr chain (Fig. S1 and S2, ESI†). The Ag(I)-hydrogels are soluble in both DMF and DMSO and insoluble in water and common organic solvents (alcohol, acetonitrile, acetone,

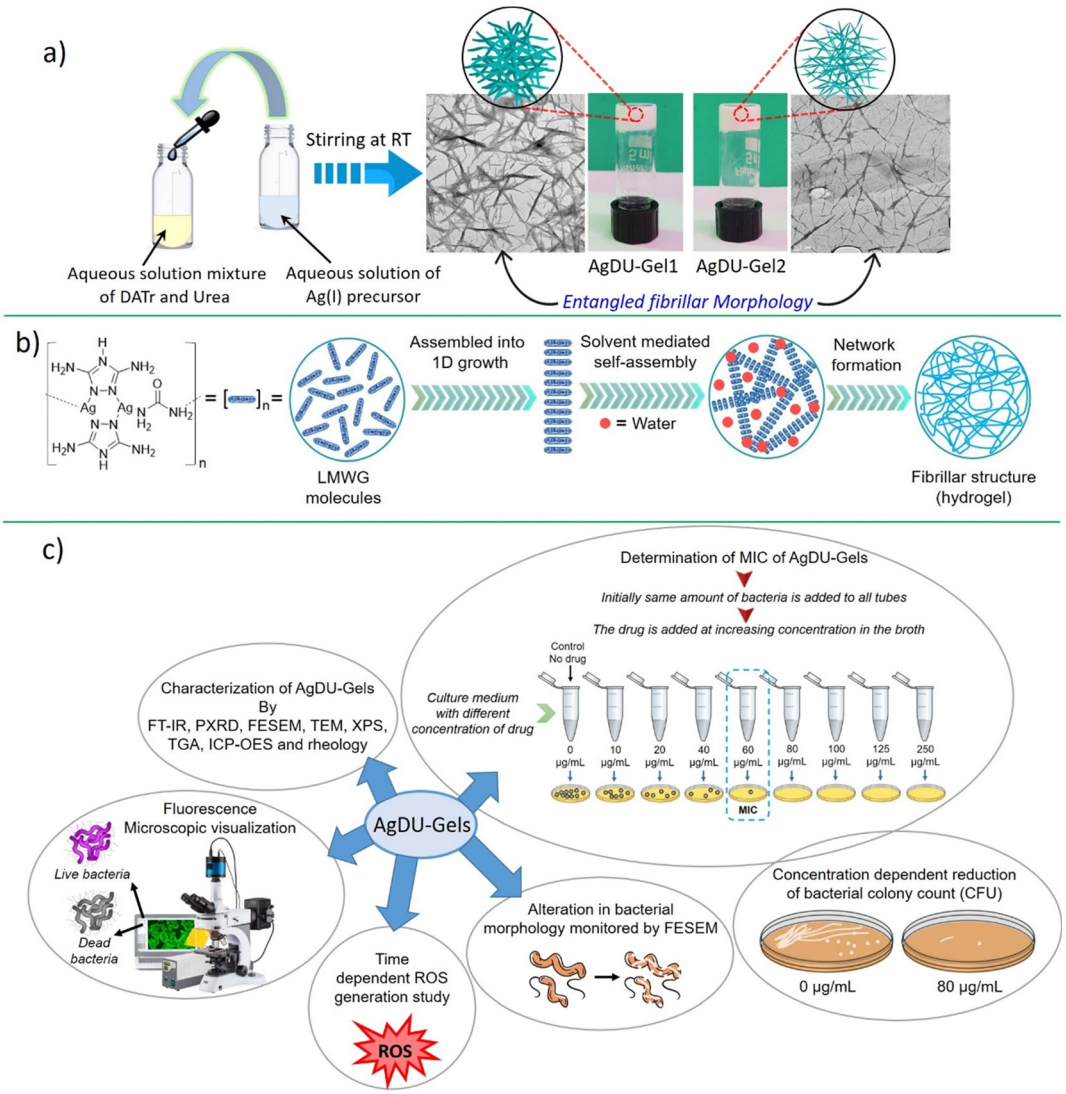

Fig. 1 (a) The synthetic scheme of the metallogels and photographs of the metallogels **AgDU-Gel1** and **AgDU-Gel2**, (b) schematic representation of the probable basic unit of AgDU-Gels and its self-assembly mechanism affording gelation and (c) assessment of the antibacterial potential of AgDU-Gels.

chloroform). Lyophilization of the hydrogels **AgDU-Gel1** and **AgDU-Gel2** resulted in the corresponding xerogels, **AgDU-Xero1** and **AgDU-Xero2**, respectively. The minimum gelator concentration (MGC) was evaluated at 0.15 and 0.125 mmol, respectively, for the hydrogels **AgDU-Gel1** and **AgDU-Gel2** (Fig. S3, ESI†).

Fourier transform infrared (FT-IR) spectroscopy of the gels and xerogels (Fig. S4, ESI†) provided insights into the gelation phenomena and the role of hydrogen bonding in gelation. The –NH (ring nitrogen) band merged with the amine (exocyclic) bands in the gels (and xerogels), and the $-NH_2$ bands shifted to $\sim$3332 cm^{-1} and $\sim$3133 cm^{-1} in the hydrogels and corresponding xerogels, respectively, indicating the participation of $-NH_2$ groups in hydrogen bonding during gelation and the removal of solvent molecules in the xerogels.[37] The bands attributed to C=N and N=N at $\sim$1500–1580 cm^{-1} remained almost unchanged in the xerogels. A new band at $\sim$412–414 cm^{-1} in the gels (and xerogels) was assigned to ν_{Ag-N}, and supported the coordination of Ag(I) with the triazole ring nitrogens.[38] The analogous FT-IR bands of the hydrogels and the corresponding xerogels indicate that the internal structure of the gels was retained in the xerogels.

PXRD analysis (Fig. 2) of the Ag(I)-based hydrogels and their corresponding xerogels suggested an ordered crystalline structure. The peak at $\sim 2\theta = 29^\circ$ (d-spacing of 3.09 Å) confirms the presence of metal–metal interactions, while $\sim 2\theta = 13.99^\circ$ (d-spacing of 6.0–6.3 Å) indicates the stacking distance of the Ag(I)-DATr moieties.[39] Peaks around $\sim 2\theta = 45.6^\circ$ (d-spacing of 1.98 Å) endorsed the presence of hydrogen bonds.[39,40] The slight shifts observed in the 2θ values of the PXRD patterns of **AgDU-Gel(Xero)1** and **AgDU-Gel(Xero)2** can be attributed to changes in the hydrogen bonding interactions, and lattice packing in the corresponding systems owing to the differing counter anions, *i.e.* triflate in **AgDU-Gel(Xero)1** and nitrate in **AgDU-Gel(Xero)2**. The scope, geometry, strength, and directionality of hydrogen bonding interactions with anions depend on the nature of the counteranions. Generally, the triflate anion is considered as sterically bulky, and a weaker hydrogen bond acceptor compared to nitrate anion, which is a relatively stronger hydrogen bond acceptor.

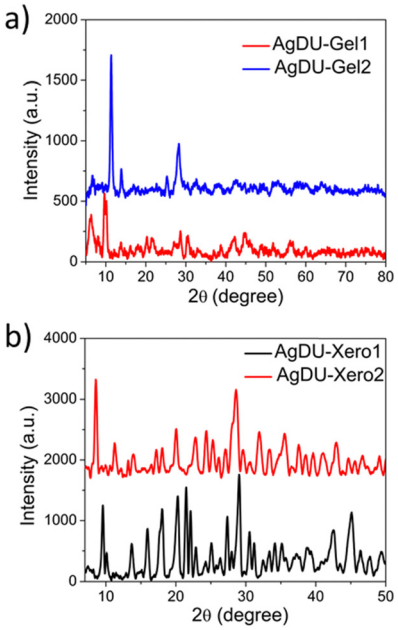

Fig. 2 PXRD profiles of the gels (and corresponding xerogels). (a) **AgDU-Gel1** and **AgDU-Gel2**; (b) **AgDU-Xero1** and **AgDU-Xero2** respectively.

Rheological analysis

Rheology is the defining characteristic of supramolecular gels, and is used to assess the mechanical properties of the as-synthesized gel samples.[41] Rheological measurements (amplitude and frequency sweeps) indicated the viscoelastic nature of both the hydrogels **AgDU-Gel1** and **AgDU-Gel2**, as the storage modulus (G') and the loss modulus (G'') remained virtually constant at low strain regions, and the storage modulus (G') was higher than the loss modulus (G''). The amplitude sweep experiments displayed a broad linear viscoelastic (LVE) region at a constant frequency (1 rad s^{-1}) with a gradual increase in the amplitude of oscillations (strain %), below a critical strain (Fig. 3a and d). At higher imposed strain, a deviation from linearity was observed due to a strain-induced weakening of the gel network. The crossover between the G' and G'' beyond the critical strain indicated a collapse of the gel network and a gel-to-sol transformation (Fig. 3a and d). The critical strain observed for **AgDU-Gel1** and **AgDU-Gel2** was 8.16% and 21.17%, respectively. These results suggested that the nitrate-containing hydrogel **AgDU-Gel2**, is more organized and robust compared to the triflate containing **AgDU-Gel1**. The higher elasticity and rigidity of **AgDU-Gel2** compared to **AgDU-Gel1** was further supported by the higher magnitude of storage modulus (G') of **AgDU-Gel2** compared to **AgDU-Gel1**. Frequency sweep experiments performed at a constant amplitude of strain (0.1%) exhibited a frequency-invariant behaviour for both the hydrogels over the applied frequency range (Fig. 3b and e). In addition, the higher magnitude of G' over G'' for both the hydrogels substantiated their elastic nature. Time-dependent step-strain experiments were carried out at a constant frequency of 1 rad s^{-1} by varying the strain % from low to high beyond the critical strain and *vice versa*, allowing sufficient time (5 min) to disintegrate (gel-to-sol, *i.e.*, $G'' > G'$) and re-form (sol-to-gel, *i.e.*, $G' > G''$) the hydrogen bond-mediated gel network for both the hydrogels (Fig. 3c and f). Interestingly, the original strengths (here G') of the metallogels were regained quickly when the breaking strain was removed and a much lower strain (0.1%) was applied. **AgDU-Gel1** and **AgDU-Gel2** recovered 93.09%, and 79.25%, respectively, of their initial strength immediately after the second cycle. Even after six consecutive cycles, **AgDU-Gel1** and **AgDU-Gel2** were able to recover 78.38%, and 58.12% of their original stiffness, respectively, indicating a rapid thixotropic self-healing ability of the gels.

Field emission scanning electron microscopy (FE-SEM) and transmission electron microscopy (TEM) (Fig. 4a–d) images of the metallogels were recorded in order to understand the microstructure of the self-assembled gels. The FE-SEM of

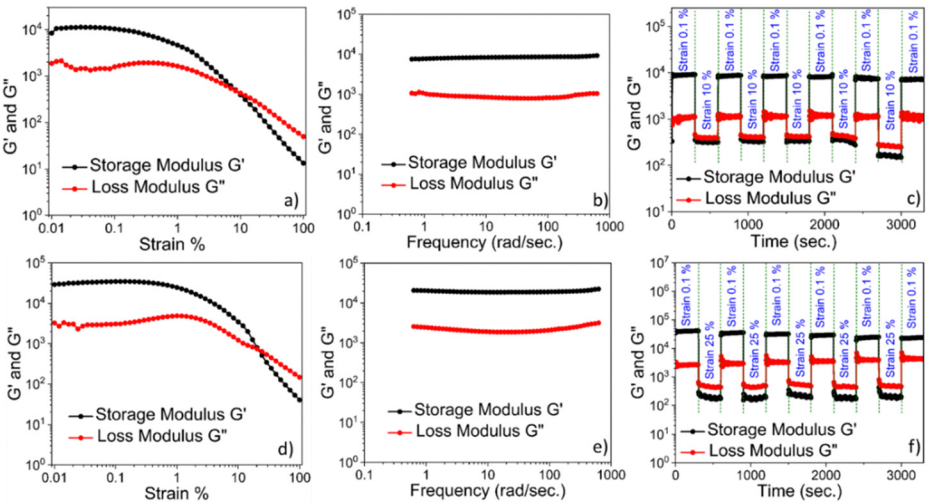

Fig. 3 Rheological measurements for the metallogels **AgDU-Gel1** and **AgDU-Gel2**. (a) and (d) represent the amplitude sweep, (b) and (e) represent the frequency sweep at constant strain and (c) and (f) represent the step-strain measurements for **AgDU-Gel1** and **AgDU-Gel2**, respectively.

AgDU-Gel1, and **AgDU-Gel2** afforded an entangled fibrillar morphology (Fig. 4a and b). Similarly, fibres of xerogels **AgDU-Xero1** and **AgDU-Xero2** were revealed from FE-SEM (Fig. S5 and S6, ESI†). The TEM images of the hydrogels **AgDU-Gel1**, and **AgDU-Gel2** corroborated the intertwined fibrous morphology observed from SEM analysis (Fig. 4c and d). TEM images of the xerogels also endorsed the fibrillar morphology (Fig. S7 and S8, ESI†).

X-ray photoelectron spectroscopy (XPS) of the xerogel samples **AgDU-Xero1** and **AgDU-Xero2** ascertained the oxidation state of Ag and the chemical composition of the xerogels. The survey spectrum revealed the presence of Ag, C, N, O, S and F for **AgDU-Xero1** and Ag, C, N and O for **AgDU-Xero2** (Fig. 4e and g). Two well-resolved peaks at binding energies ~369 and ~375 eV corresponding to Ag $3d_{5/2}$ and Ag $3d_{3/2}$ with a spin–orbit separation of ~6 eV supported the presence of Ag(I) in both the xerogels (Fig. 4f and h).[42,43] The C 1s signal of **AgDU-Xero1** was deconvoluted to reveal sp^2/sp^3 carbon, C–N/C═O and C–F (corresponding to the triflate counter anion) at binding energies 284.90, 288.0 and 292.80 eV, respectively (Fig. S9a, ESI†). Similar carbon species were present in **AgDU-Xero2**, except for the C–F functionality, which was absent in **AgDU-Xero2** (Fig. S10a, ESI†). The N 1s spectrum states the presence of C–N/C═N/Ag–N, and N–H at 399.85 (399.48) and 400.61 (400.23) eV, respectively, for **AgDU-Xero1** (and **AgDU-Xero2**). An additional peak at 406.82 eV appears due to the nitrate counter anion in **AgDU-Gel2** (Fig. S9b and S10b, ESI†).[42] The O 1s spectra confirm the presence of C═O and adsorbed moisture (water/OH^-) at 532.40 and

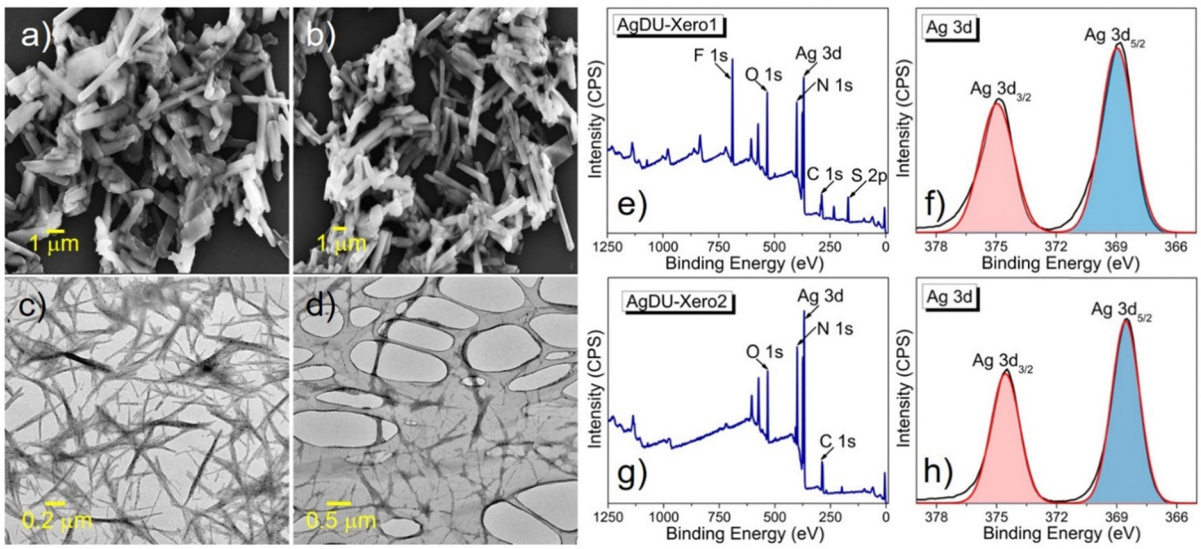

Fig. 4 FE-SEM images of the gels (a) **AgDU-Gel1**, and (b) **AgDU-Gel2**. Corresponding TEM images of the gels are presented in (c) **AgDU-Gel1**, and (d) **AgDU-Gel2**, respectively, attesting to the fibrillar morphology. (e) and (g) present the XPS survey spectra of **AgDU-Gel1** and **AgDU-Gel2**, respectively, and their corresponding high-resolution Ag 3d traces are presented as (f) and (h), respectively.

534.28 eV, respectively, for both the xerogels (Fig. S9c and S10c, ESI†). An almost similar surface elemental analysis was recorded for both the xerogels (Fig. S11, ESI†).

Stimuli-responsive nature of AgDU-Gel1 and AgDU-Gel2

Changes in the hydrogel **AgDU-Gel1** were monitored in the presence of a gamut of physical and chemical external stimuli. **AgDU-Gel1** remained unaltered on prolonged sonication for 2 h and when heated in a water bath (Fig. S13, ESI†). The thermal stability of the AgDU-hydrogels was substantiated by TGA profiles (Fig. S12, ESI†), which showed the thermal stability of the materials up to ~150 °C. *Gel-to-sol* conversion was observed with alkali metal halides except for fluoride, which could not disintegrate the gel network, presumably owing to the reduced solubility of LiF in water (Fig. S13, ESI†). **AgDU-Gel1** collapsed in the presence of oxyanions owing to a disturbance of the hydrogen-bonded network or metal–ligand coordination environment constituting the gel (Fig. S13, ESI†). Na_2SO_4 (SO_4^{2-}) was ineffective in disrupting the gel network. We surmise that the retention of the gel network in the presence of SO_4^{2-} ions could be because SO_4^{2-} is a strong hydrogen bond acceptor, and is known for its strong coordination capacity to metal ions.[44] The disruption of the gel network in the presence of SO_4^{2-} is rarely observed for gels. The pH-responsive nature of the hydrogels was ascertained in the presence of both acids and bases. The gel nature in the hydrogel **AgDU-Gel1** was lost upon the addition of 100 μL each of 1(M) hydrochloric acid (HCl), glacial acetic acid (AcOH), liquor ammonia (NH_3) and NaOH solution (Fig. S13, ESI†). The disintegration of the gel network in the AcOH-treated gel is due to the formation of silver acetates (Fig. S13, ESI†). The addition of a few drops (100 μL) of 0.5(M) ethylenediaminetetraacetic acid (EDTA) solution (pH ~8) to the gel resulted in a disintegration in the gel due to the formation of white precipitates of silver–EDTA complex, *i.e.* Ag_4Y species (EDTA anion is Y^{4-}) with a clear sol (Fig. S13, ESI†). Tetrabutylammonium bromide (TBABr) was found to disrupt the AgDU-gel network, as the bulky cation and anion aided in weakening the hydrogen-bonded network. The sol thus formed underwent re-gelation upon the addition of excess $AgNO_3$, which effectively scavenged the Br^- by forming a AgBr precipitate, thus restoring the hydrogen-bonded gel network (Fig. S13, ESI†). A similar multi-stimuli responsive nature was observed for **AgDU-Gel2** (Fig. S14, ESI†).

It is reported that positive charge on materials benefits their bactericidal ability by facilitating the perturbation of the negatively charged cell membrane, resulting in the development of amphiphiles and antimicrobial peptides for their antibacterial efficacy.[19,45,46] Zeta potential measurements for the xerogels **AgDU-Xero1** and **AgDU-Xero2** disclosed a positive charge of +18.1 mV and +17.4 mV, respectively (Table S2, ESI†), confirming the overall positively charged surface. Ag(I)-hydrogels with the prominent presence of pendant $-NH_2$ groups are expected to enhance their reactivity *via* hydrogen-bond formation with the bacterial membrane.[47] In view of the bactericidal effects of Ag(I) species, the purpose-built multicomponent supramolecular Ag(I)-hydrogel with $-NH_2$ groups, and positive surface charge were explored as a broad-spectrum antimicrobial candidate against both Gram-positive *S. aureus* (MRSA) and Gram-negative *C. jejuni*.

Cell cytotoxicity and biocompatibility of the AgDU-Xerogels

To determine the cytotoxic effect of **AgDU-Xerogels**, the 50% cytotoxic concentration (CC_{50}) was calculated by a standard 3-(4,5-dimethylthiazol-2-yl)-2,5-diphenyl tetrazolium bromide (MTT) assay. Human Caco-2 cells, HEK293T and INT407 cells were treated with different concentrations of **AgDU-Xerogels** (ranging from 0 μg mL^{-1} to 250 μg mL^{-1}) and incubated for 24 h. The CC_{50} value of **AgDU-Xero1** is ~33 μg mL^{-1} for Caco-2, ~13.3 μg mL^{-1} for HEK293T and ~6.4 μg mL^{-1} for INT407. The CC_{50} value of **AgDU-Xero2** is ~27 μg mL^{-1} for Caco-2, ~14 μg mL^{-1} for HEK293T and ~4.4 μg mL^{-1} for INT407 (Fig. S15, ESI†).

Cytotoxicity data indicate that AgDU-xerogels as a multi-composite formulation have some cytotoxic effects in human cells. The AgDU-xerogel is composed of DATr, Urea, and $AgNO_3$/AgOTf, which are intrinsically cytotoxic;[48–54] hence as a composite, it is expected that our multi-composite xerogels would also exhibit some cell cytotoxicity. However, considering the intended application of the present supramolecular xerogels as antibacterial coatings on inanimate objects and not for *in vivo* use, biocompatibility may not be a concern.

Antibacterial activity against MRSA and *C. jejuni*

The antibacterial activity of Ag(I)-hydrogel-derived xerogels **AgDU-Xero1** and **AgDU-Xero2** was evaluated against drug-resistant Gram-positive and Gram-negative pathogens. To determine the MIC_{50} of the test materials on bacterial growth, the bacterial viability was plotted individually for **AgDU-Xero1** and **AgDU-Xero2**, as shown in Fig. 5. The MIC was determined by the micro-broth dilution method.[55] The mean absorbance (OD_{600nm}) of the bacterial growth in the presence of xerogels (at different concentrations starting from 0 to 250 μg mL^{-1}) was measured to calculate the bacterial viability. The data suggested that the MIC_{50} value for both types of xerogels is ~60 μg mL^{-1} against MDR *C. jejuni* (Fig. 5a) and ~ 62.5 μg mL^{-1} against MRSA (Fig. 5b, Table S3, ESI†), which compared favourably with reported antibacterial formulations against *C. jejuni* and MRSA (Table S4 and S5, ESI†). As a control, bacteria grown without test compounds showed no changes in bacterial growth. Based on the MIC value, the xerogel loadings chosen for subsequent antibacterial studies were 40, 60, and 80 μg mL^{-1} for both bacteria.

Concentration-dependent reduction of bacterial growth

To determine the effect of **AgDU** xerogels, bacterial cells were co-incubated with **AgDU-Xero1** and **AgDU-Xero2** for 5 h at 37 °C and plated on the respective selective agar medium. For both test compounds, bacterial counts (colony forming unit; CFU) were found to be reduced in a concentration-dependent manner for both *C. jejuni* (Fig. 6a and b) and *S. aureus* (Fig. 6c and d). Data suggested a significant reduction of bacterial count for both bacteria in the presence of different concentrations of **AgDU-Xero1** and **AgDU-Xero2** (ranging from 40 μg mL^{-1} to 80 μg mL^{-1}). **AgDU-Xero2** showed better efficacy in restricting

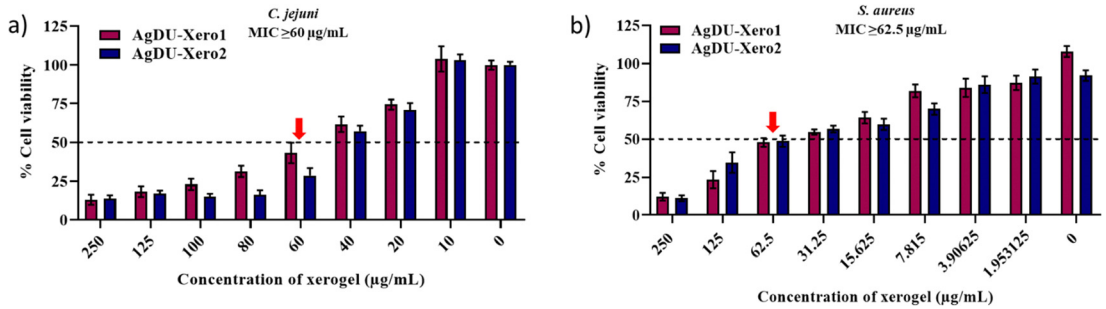

Fig. 5 Minimum inhibitory concentration (MIC) of xerogels (**AgDU-Xero1** and **AgDU-Xero2**) against *C. jejuni* and *S. aureus*. The MIC value for both xerogels is ≥ 60 μg mL^{-1} against *C. jejuni* (a) and ≥ 62.5 μg mL^{-1} for both compounds against *S. aureus* (b).

C. jejuni growth than **AgDU-Xero1**, while **AgDU-Xero1** and **AgDU-Xero2** portrayed similar efficacy against *S. aureus*. Also, as a multi-component formulation, AgDU-xerogels used herein showed a marked reduction in bacterial growth compared to the individual components (such as DATr, Urea, and $AgNO_3$/AgOTf) (Fig. S16, ESI†). The superposition of the activity of the individual components, in addition to the abundance of primary amine groups in both urea and DATr, which are envisaged to exhibit synchronized non-covalent interactions, enhances the likelihood of the composite hydrogel interacting with bacterial membranes extensively *via* hydrogen bonding, leading to an improvement in the antimicrobial activity.

Enhanced cell death and generation of reactive oxygen species (ROS) due to AgDU-Xero1 and AgDU-Xero2 treatment of bacteria

To investigate the bactericidal activity of **AgDU-Xero1** and **AgDU-Xero2**, a double-staining method was applied using 4′,6-diamidino-2-phenylindole (DAPI) and propidium iodide (PI) dyes (Fig. 7) based on the principle that DAPI stains all bacterial cells irrespective of their viability, while PI, a cell-impermeable dye, only stains the nucleic acid of membrane-compromised cells. Bacterial cells were incubated with three concentrations (40 μg mL^{-1}, 60 μg mL^{-1}, and 80 μg mL^{-1}) of the xerogels for 5 h and imaged under a confocal laser scanning microscope.

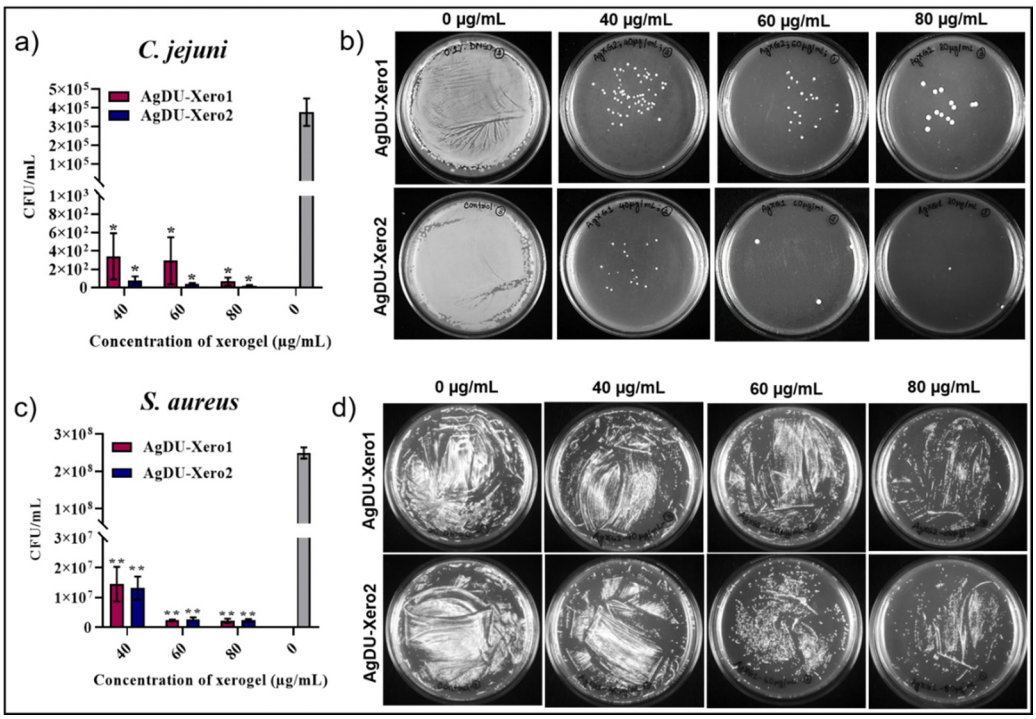

Fig. 6 Antibacterial activity of **AgDU-Xero1** and **AgDU-Xero2** against *C. jejuni* and *S. aureus*. Both bacteria were cultured in an increasing concentration of xerogels (40 μg mL^{-1}, 60 μg mL^{-1} and 80 μg mL^{-1}). After incubation for 5 h, approximately 50 μL from each set was plated on the respective agar media. The resulting colonies were counted, and CFU was calculated as per the following formula: CFU/mL = (No. of colonies × Total dilution factor)/(Volume of culture plated in mL). The data are presented as mean ± SE from three independent experiments. The count (CFU mL^{-1}) of *C. jejuni* (a) and *S. aureus* (c) after being treated with **AgDU-Xero1** and **AgDU-Xero2**, respectively. Representative plate images of recultivated bacterial colonies appeared on the MH agar plate of *C. jejuni* (b) and the LB agar plate of *S. aureus* (d). Data suggest that the CFU counts decreased with the increment of the drug concentration.

Bacterial cells without test compounds were treated as a control, and marked with green (pseudocolor) due to DAPI staining. No red emission could be detected due to PI-staining in the control cells, confirming that the bacterial membrane was intact and the bacteria were largely alive. The images captured for *C. jejuni* (Fig. 7a) and *S. aureus* (Fig. 7b) incubated with **AgDU-Xero1** and **AgDU-Xero2** displayed green color (for DAPI stained nucleus) as well as strong red emissions (from PI), which corroborates the bacterial membrane disruption due to **AgDU-Xero1** and **AgDU-Xero2** treatment. The merged images show the co-localization of both DAPI and PI. Next, we investigated the effect of **AgDU-Xero1** and **AgDU-Xero2** to facilitate the ROS generation using 2′,7′-dichlorodihydrofluorescein diacetate (H_2DCFDA) dye. A critical analysis suggests that the intracellular ROS generation induced by **AgDU-Xero1** and **AgDU-Xero2** is time-dependent (Fig. 7c and d). With a function of time, ROS production increased up to 1 h of incubation with the test compounds for both the bacteria. After 2 h of incubation with the test compounds, ROS generation was decreased. However, it remained higher than that observed for the controls. Thus, the data suggested that the fatal distress causing bacterial cell death mediated by the Ag(I)-xerogels was aided by the involvement of ROS.

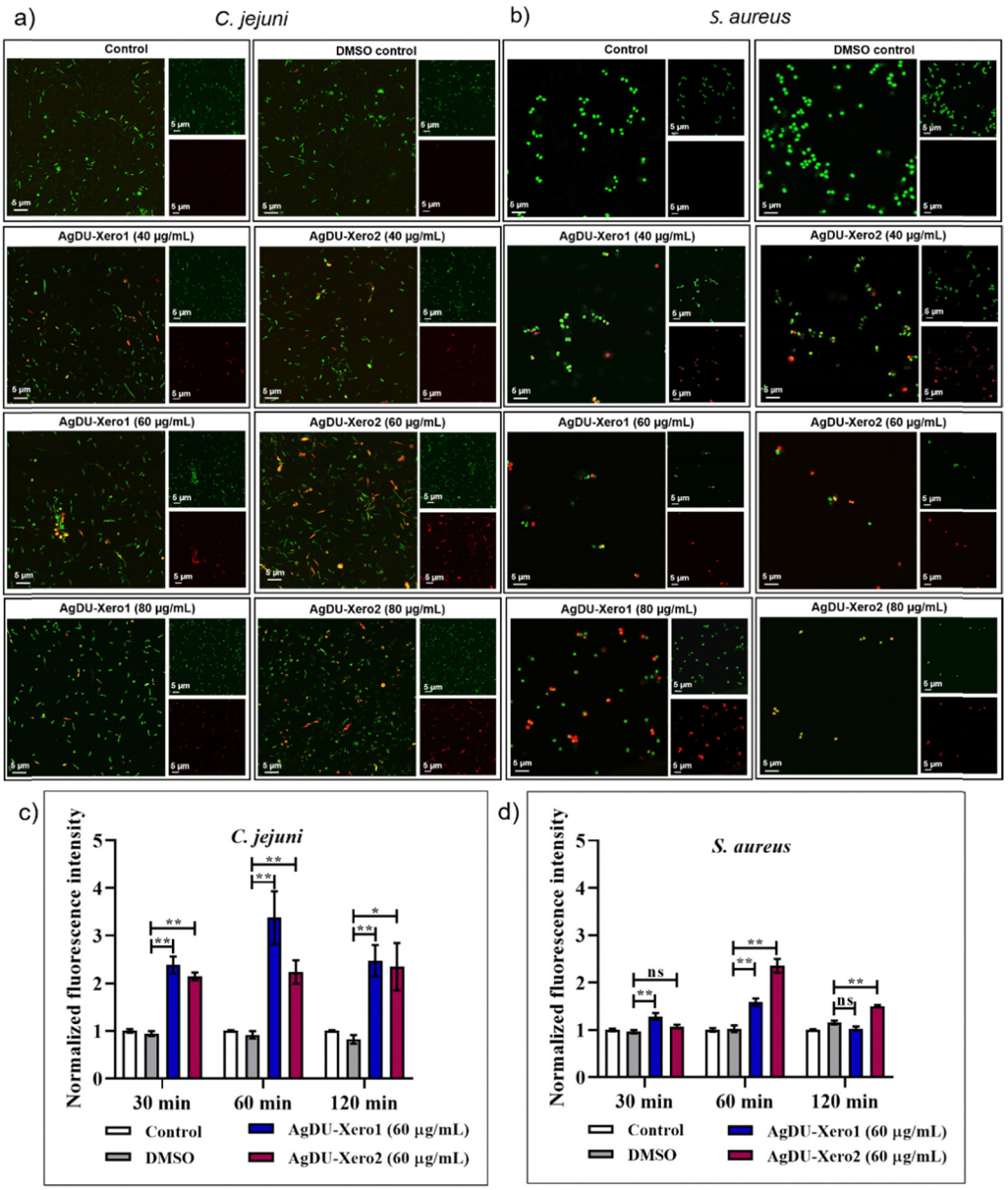

Fig. 7 Representative fluorescence microscopy images of *C. jejuni* (a) and *S. aureus* (b) incubated with **AgDU-Xero1** and **AgDU-Xero2**. The cells were stained by DAPI (green) and PI (red) [Incubation time = 5 h]. The green colour represents live + dead bacteria, whereas red only represents dead bacteria. Reactive Oxygen Species (ROS) induced in bacteria treated with **AgDU-Xero1** and **AgDU-Xero2**. Quantification of total ROS Generation in *C. jejuni* (c) and *S. aureus* (d) in the presence of xerogels.

Changes in membrane integrity and morphology of bacterial cells triggered by AgDU-Xero1 and AgDU-Xero2

To visualize the effect of **AgDU-Xero1** and **AgDU-Xero2** treatment on bacterial cells, FE-SEM was performed. For this, bacterial cells were co-incubated with or without the test compounds for 5 h, processed for FE-SEM and the images were captured. While untreated *C. jejuni* cells (control) show a natural spiral shape with smooth, continuous, and unbroken cell membranes, the cells treated with **AgDU-Xero1** and **AgDU-Xero2** resulted in marked changes in morphology and compromised membrane integrity with the prominent presence of holes in the bacterial membrane (Fig. 8a). A similar observation was recorded in the case of *S. aureus* when treated with **AgDU**-xerogel, displaying shrinking and disruption of the bacterial cell membrane, in contrast to the smooth spherical shape in control cells (Fig. 8b).

We surmise that the cumulative effect of extensive hydrogen bonding interactions due to the predominance of pendant $-NH_2$ groups and the positive surface potential in Ag(I)-xerogels (Table S2, ESI†) culminate in disrupting the negatively charged phospholipid bilayer of the bacterial cells (Fig. 9).[46,56] This results in the ejection of the cellular content which, in conjunction with sustained ROS generation, causes bacterial cell death. Electrostatic interactions between cationic **AgDU**-xerogels and anionic phospholipid bilayers of the bacterial cell membrane play a pivotal role in the bactericidal response of the xerogels in addition to hydrogen bonding, hydrophobic and ionic interactions.[57] The physiologically demanding repair of bacterial cell membranes is one of the reasons for positively charged species developing less antimicrobial resistance.[8,58] Generally, most antibacterial agents show high efficacy against Gram-positive bacteria; however, they often prove less effective against Gram-negative bacteria due to the presence of the additional protection afforded by the outer membrane.[59,60] Interestingly, our data suggest comparable efficacy of the multicomponent Ag(I)-xerogels against Gram-negative and Gram-positive bacteria.

Given that the counter anions play a significant role in altering the antimicrobial activity of the common antibacterial formulations,[61] in our case, **AgDU-Xero1** and **AgDU-Xero2** showed a similar MIC_{50} value ($\sim$60 μg mL^{-1}), indicating no significant changes in their activity. However, in terms of differential activity, we found that the antibacterial effect of **AgDU-Xero2** is more prominent than **AgDU-Xero1**. We surmise that the reduced antimicrobial activity of **AgDU-Xero1** compared to **AgDU-Xero2** is possibly due to poor hydrogen bonding ability of the triflate counter anion present in the former, compared to the nitrate counter anion in **AgDU-Xero2**. The CF_3 group in triflate localizes its charge density, affecting its overall charge distribution and consequently its ability to participate in hydrogen bond formation. In contrast, the nitrate counter anion is more available towards the formation of H-bonds through the oxygen atoms.[62] In addition, the comparatively lower antimicrobial activity of **AgDU-Xero1** than **AgDU-Xero2** against *C. jejuni* could presumably be due to the poor release of silver and low availability of antibacterial silver ions. Therefore, we propose that the antimicrobial activity of the studied multicomponent Ag(I)-hydrogel-derived xerogels is influenced not only by the activity of the Ag–DATr–Urea complex ion but also by the counter ion X^- (NO_3^- or $CF_3SO_3^-$), though a conclusive trend has not been identified regarding the

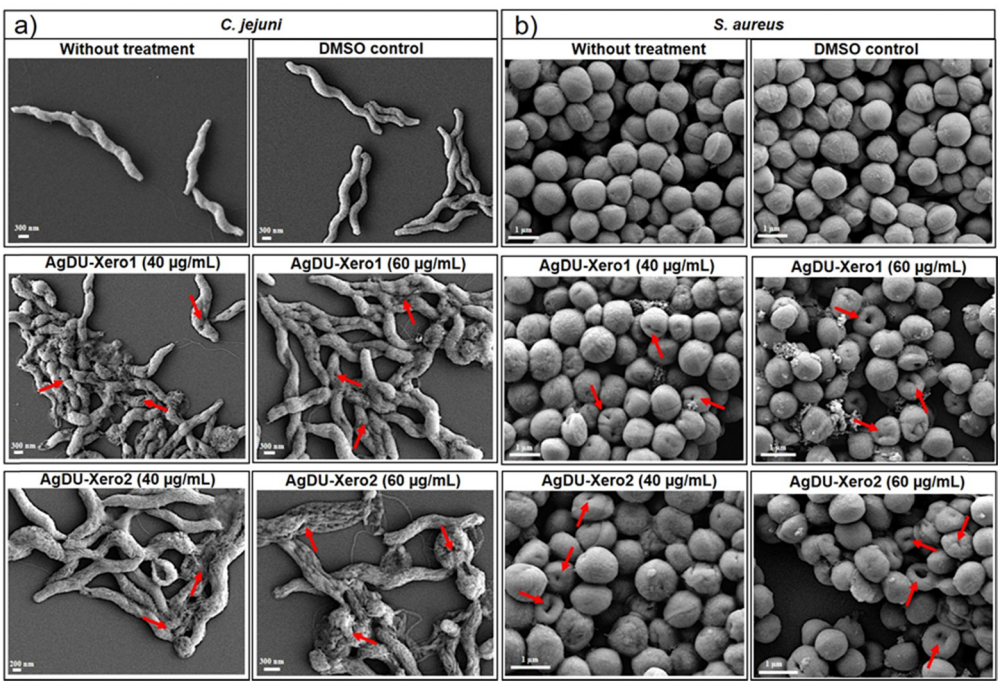

Fig. 8 Changes in bacterial morphology after treatment with **AgDU-Xero1** and **AgDU-Xero2**. Distinct changes in *C. jejuni* (a) and *S. aureus* (b) morphology in the presence of **AgDU-Xero1** and **AgDU-Xero2**, respectively, were observed under FE-SEM. The red arrows indicate morphological changes of *C. jejuni* and *S. aureus* cells, respectively. Scale bar: 300 nm (*C. jejuni*) and 1 μm (*S. aureus*).

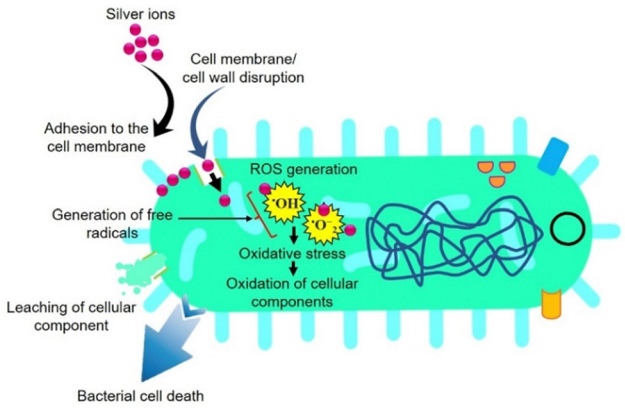

Fig. 9 Schematic of the mechanism of antibacterial action of the **AgDU**-Xerogels.

utility of a certain counter anion towards antimicrobial activity, compared to other counter anions.[63,64]

Thus, our results delineate the potential of multicomponent Ag(I)-hydrogels (and derived xerogels **AgDU-Xero1** and **AgDU-Xero2)** as future alternatives to antibiotics in treating a broad-spectrum of MDR pathogens.

Conclusions

The present study highlights the potential benefit of carefully fabricated Ag(I)-hydrogels using DATr and urea ligands as broad-spectrum antibacterial agents against drug-resistant "hard-to-treat" bacterial pathogens. Our experimental evidence suggests that the multicomponent Ag(I)-hydrogels could be a promising candidate for controlling MDR and ESKAPE pathogens. The cumulative effect of a positively charged hydrogel system with Ag(I) and pendant $-NH_2$ groups on the gelators facilitates multiple hydrogen bonding interactions with the negatively charged bacterial cell membrane resulting in an enhanced antibacterial activity due to the disintegration of the bacterial membrane and intracellular ROS generation in multi-drug-resistant bacteria, *C. jejuni* and MRSA. We propose that these materials can improve the antibacterial efficacy of known antibiotics, thus revitalizing the treatment of MDR bacterial infections.

Author contributions

ES: methodology, formal analysis, data curation (synthesis & characterization of hydrogels), validation, writing – review & editing. AK: methodology, formal analysis, data curation (antibacterial experiments), validation, writing – review & editing. AIM: Fund acquisition, supervision (AK), writing – review & editing. JM: Fund acquisition, supervision (ES), writing – review & editing. All authors have read and approved the final manuscript.

Data availability

The data supporting this article have been included as part of the ESI.†

Conflicts of interest

The authors declare no competing financial interest.

Acknowledgements

The authors thank AESD&CIF, CSIR-CSMCRI and IISER Kolkata for instrumental facilities. We acknowledge the Central Electron Microscopy Facility, IISER Kolkata, for the FE-SEM. AK and AIM acknowledge support from IISER Kolkata. ES thanks the DST-INSPIRE Fellowship for financial support. JM acknowledges SERB POWER Grant SPG/2021/004430 for funding. AK thanks the UGC, MoE, Govt. of India for fellowship support. This work is supported by the Department of Biotechnology, Govt. of India (Grant no. BT/PR40625/AAQ/1/799/2020) to AIM. CSMCRI manuscript PRIS No. 150/2023.

Notes and references

1 C. J. L. Murray, K. S. Ikuta, F. Sharara, L. Swetschinski, G. Robles Aguilar, A. Gray, C. Han, C. Bisignano, P. Rao, E. Wool and S. C. Johnson, *Lancet*, 2022, **399**, 629.
2 E. M. Darby, E. Trampari, P. Siasat, M. S. Gaya, I. Alav, M. A. Webber and J. M. Blair, *Nat. Rev. Microbiol.*, 2023, **21**(5), 280.
3 G. M. Knight, R. E. Glover, C. F. McQuaid, I. D. Olaru, K. Gallandat, Q. J. Leclerc, N. M. Fuller, S. J. Willcocks, R. Hasan, E. van Kleef and C. I. Chandler, *eLife*, 2021, **10**, e64139.
4 J. G. Hurdle, A. J. O'Neill, I. Chopra and R. E. Lee, *Nat. Rev. Microbiol.*, 2011, **9**, 62.
5 D. S. S. M. Uppu, M. M. Konai, U. Baul, P. Singh, T. K. Siersma, S. Samaddar, S. Vemparala, L. W. Hamoen, C. Narayana and J. Haldar, *Chem. Sci.*, 2016, **7**, 4613.
6 S. Kumar, J. Thakur, K. Yadav, M. Mitra, S. Pal, A. Ray, S. Gupta, N. Medatwal, R. Gupta, D. Mishra, P. Rani, S. Padhi, P. Sharma, A. Kapil, A. Srivastava, U. D. Priyakumar, U. Dasgupta, L. Thukral and A. Bajaj, *ACS Biomater. Sci. Eng.*, 2019, **5**, 4764.
7 M. Le, W. Huang, Z. Ma, Z. Shi, Q. Li, C. Lin, L. Wang and Y.-G. Jia, *Biomacromolecules*, 2023, **24**, 269.
8 B. Hu, C. Owh, P. L. Chee, W. R. Leow, X. Liu, Y. L. Wu, P. Guo, X. J. Loh and X. Chen, *Chem. Soc. Rev.*, 2018, **47**(18), 6917.
9 J. Miao, X. Wu, Y. Fang, M. Zeng, Z. Huang, M. Ouyang and R. Wang, *J. Mater. Chem. B*, 2023, **11**, 3373–3386.
10 D. Bursy, R. Balwierz, P. Groch, P. Biernat, A. Byrski, K. Kasperkiewicz and W. Ochędzan-Siodłak, *Pharmacol. Rep.*, 2023, **75**(3), 657–670.
11 B. J. Nablo, H. L. Prichard, R. D. Butler, B. Klitzman and M. H. Schoenfisch, *Biomaterialia*, 2005, **26**(34), 6984–6990.
12 C. Zhao, L. Zhou, M. Chiao and W. Yang, *Adv. Colloid Interface Sci.*, 2020, **285**, 102280.
13 H. Nabipour, X. Wang, M. Z. Rahman, L. Song and Y. Hu, *J. Cleaner Prod.*, 2020, **273**, 122832.
14 F. Bamba, T. Camara, C. Sioménan, S. J. Akpa and A. Ané, *Adv. Biochem.*, 2021, **9**(4), 98.

15 K. Pandurangan, J. A. Kitchen, S. Blasco, F. Paradisi and T. Gunnlaugsson, *Chem. Commun.*, 2014, **50**(74), 10819.
16 P. S. Charifson, A. L. Grillot, T. H. Grossman, J. D. Parsons, M. Badia, S. Bellon, D. D. Deininger, J. E. Drumm, C. H. Gross, A. LeTiran and Y. Liao, *J. Med. Chem.*, 2008, **51**(17), 5243.
17 J. Wang, B. Li, X. Pu, X. Wang, R. C. Cooper, Q. Gui and H. Yang, *ACS Appl. Mater. Interfaces*, 2020, **12**(9), 10202.
18 G. Dhanda, R. Mukherjee, D. Basak and J. Haldar, *ACS Infect. Dis.*, 2022, **8**, 1086.
19 A. Dey, M. Yadav, D. Kumar, A. K. Dey, S. Samal, S. Tanwar, D. Sarkar, S. K. Pramanik, S. Chaudhuri and A. Das, *Chem. Sci.*, 2022, **13**(34), 10103.
20 T. C. Dakal, A. Kumar, R. S. Majumdar and V. Yadav, *Front. Microbiol.*, 2016, **7**, 1831.
21 M. He, Q. Wang, J. Zhang, W. Zhao and C. Zhao, *ACS Appl. Mater. Interfaces*, 2017, **9**(51), 44782.
22 C.-N. Lok, C.-M. Ho, R. Chen, Q.-Y. He, W.-Y. Yu, H. Sun, P. K.-H. Tam, J.-F. Chiu and C.-M. Che, *J. Biol. Inorg. Chem.*, 2007, **12**, 527.
23 S. Chernousova and M. Epple, *Angew. Chem., Int. Ed.*, 2013, **52**(6), 1636.
24 I. L. Hsiao, Y. K. Hsieh, C. F. Wang, I. C. Chen and Y. J. Huang, *Environ. Sci. Technol.*, 2015, **49**(6), 3813.
25 F. Xu, H. Padhy, M. Al-Dossary, G. Zhang, A. R. Behzad, U. Stingl and A. Rothenberger, *J. Mater. Chem. B*, 2014, **2**(37), 6406.
26 L. Qin, P. Wang, Y. Guo, C. Chen and M. Liu, *Adv. Sci.*, 2015, **2**(11), 1500134.
27 J. Keithlin, J. Sargeant, M. K. Thomas and A. Fazil, *BMC Public Health*, 2014, **14**, 1203.
28 Y. Tang, R. J. Meinersmann, O. Sahin, Z. Wu, L. Dai, J. Carlson, J. Plumblee Lawrence, L. Genzlinger, J. T. LeJeune and Q. Zhang, *Appl. Environ. Microbiol.*, 2017, **83**(24), e01425.
29 T. Luangtongkum, B. Jeon, J. Han, P. Plummer, C. M. Logue and Q. Zhang, *Future Microbiol.*, 2009, **4**(2), 189.
30 H. Grundmann, M. Aires-de-Sousa, J. Boyce and E. Tiemersma, *Lancet*, 2006, **368**(9538), 874.
31 V. Krishnamurthy, A. Saha, B. V. Renushri and E. R. Nagaraj, *J. Clin. Diagn. Res.*, 2014, **8**(7), DC04.
32 B. A. Fomda, M. A. Thokar, A. Khan, J. A. Bhat, D. Zahoor, G. Bashir, A. Majid and P. Ray, *Indian J. Med. Microbiol.*, 2014, **32**(1), 39.
33 M. Otto, *Annu. Rev. Microbiol.*, 2010, **64**, 143.
34 R. R. Gurung, P. Maharjan and G. G. Chhetri, *Future Sci. OA*, 2020, **6**(4), FSO464.
35 S. I. Miller, *mBio*, 2016, **7**(5), e01541.
36 T. Ishida, *MOJ Toxicol*, 2018, **4**(5), 345.
37 R. M. Almotawa, G. Aljomaih, D. V. Trujillo, V. N. Nesterov and M. A. Rawashdeh-Omary, *Inorg. Chem.*, 2018, **57**(16), 9962.
38 K. A. Ali, M. M. Abd-Elzaher and K. Mahmoud, *Int. J. Med. Chem.*, 2013, **2013**, 256836.
39 W. Fang, Z. Sun and T. Tu, *J. Phys. Chem. C*, 2013, **117**(47), 25185.
40 L. Mistry, O. OsamaEl-Zubir, G. Dura, W. Clegg, P. G. Waddell, T. Pope, W. A. Hofer, N. G. Wright, B. R. Horrocksa and A. Houlton, *Chem. Sci.*, 2019, **10**, 3186.
41 E. R. Draper and D. J. Adams, *Chem. Soc. Rev.*, 2018, **47**(10), 3395.
42 A. M. Ferraria, A. P. Carapeto and A. M. B. do Rego, *Vacuum*, 2012, **86**(12), 1988.
43 S. Zhang, J. Ye, Y. Sun, J. Kang, J. Liu, Y. Wang, Y. Li, L. Zhang and G. Ning, *Chem. Eng. J.*, 2020, **390**, 124523.
44 Y. Feng, N. Jiang, D. Zhu, Z. Su and M. R. Bryce, *J. Mater. Chem. C*, 2020, **8**, 11540–11545.
45 B. Findlay, G. G. Zhanel and F. Schweizer, *Antimicrob. Agents Chemother.*, 2010, **54**(10), 4049.
46 S. Mitra, S. Kandambeth, B. P. Biswal, M. A. Khayum, C. K. Choudhury, M. Mehta, G. Kaur, S. Banerjee, A. Prabhune, S. Verma, S. Roy, U. K. Kharul and R. Banerjee, *J. Am. Chem. Soc.*, 2016, **138**(8), 2823.
47 M. Mitra, M. Asad, S. Kumar, K. Yadav, S. Chaudhary, N. S. Bhavesh, S. Khalid, L. Thukral and A. Bajaj, *J. Phys. Chem. Lett.*, 2019, **10**, 754.
48 S. M. Alsharif, S. S. Salem, M. A. Abdel-Rahman, A. Fouda, A. M. Eid, S. E. D. Hassan, M. A. Awad and A. A. Mohamed, *Heliyon*, 2020, **6**(5), e03943.
49 F. Sambale, S. Wagner, F. Stahl, R. R. Khaydarov, T. Scheper and D. Bahnemann, *J. Nanomater.*, 2015, **2015**, 136765.
50 A. Fouda, G. Abdel-Maksoud, H. A. Saad, A. A. Gobouri, Z. M. Mohammedsaleh and M. Abdel-Haleem El-Sadany, *Catalysts*, 2021, **11**(3), 310.
51 F. Hassanzadeh, H. Sadeghi-Aliabadi, S. Nikooei, E. Jafari and G. Vaseghi, *Results Pharma Sci.*, 2019, **4**(2), 130–137.
52 A. D. Glinos, G. N. Bardi, K. C. Dermitzaki, S. A. Perez and M. J. Talieri, *J. Natl. Cancer Inst.*, 1983, **71**(6), 1211–1219.
53 A. Abdelli, S. Azzouni, R. Plais, A. Gaucher, M. L. Efrit and D. Prim, *Tetrahedron Lett.*, 2021, **86**, 153518.
54 P. V. AshaRani, G. Low Kah Mun, M. P. Hande and S. Valiyaveettil, *ACS Nano*, 2009, **3**(2), 279–290.
55 H. T. P. Anh, C. M. Huang and C. J. Huang, *Sci. Rep.*, 2019, **9**, 11562.
56 J. Djafari, C. Fernández-Lodeiro, A. Fernández-Lodeiro, V. Silva, P. Poeta, G. Igrejas, C. Lodeiro, J. L. Capelo and J. Fernández-Lodeiro, *Front. Chem.*, 2019, **6**, 677.
57 A. S. Joshi, P. Singh and I. Mijakovic, *Int. J. Mol. Sci.*, 2020, **21**(20), 7658.
58 M. Le, W. Huang, Z. Ma, Z. Shi, Q. Li, C. Lin, L. Wang and Y.-G. Jia, *Biomacromolecules*, 2023, **24**, 269.
59 E. Escamilla-García, A. G. Alcázar-Pizaña, J. C. Segoviano-Ramírez, D. Angel-Mosqueda, A. P. López-Lozano, E. Cárdenas-Estrada, D. La Garza-Ramos and M. Márquez, *Int. J. Microbiol*, 2017, **2017**, 5924717.
60 R. M. Epand, C. Walker, R. F. Epand and N. A. Magarvey, *Biochim. Biophys. Acta*, 2016, **1858**(5), 980.
61 U. Kalinowska-Lis, A. Felczak, L. Chęcińska, K. Zawadzka, E. Patyna, K. Lisowska and J. Ochocki, *Dalton Trans.*, 2015, **44**, 8178.
62 N. D. Savic, B. B. Petkovic and S. Vojnovic, *Dalton Trans.*, 2020, **49**, 10880–10894.
63 M. L. Ingalsbe, J. D. S. Denis, M. E. McGahan, W. W. Steiner and R. Priefer, *Bioorg. Med. Chem. Lett.*, 2009, **19**, 4984.
64 C. M. Lee, H. J. Kim, S. Timilsina and R. Priefer, *Med. Res. Arch.*, 2022, **10**(3), DOI: **10.18103/mra.v10i3.2716**.